# Design of Maximum Power Point Tracker (MPPT) and Phase Locked Loop (PLL) in a PV-Inverter

**Ofualagba Godswill 1*, Onyan Aaron Okiemute **, Igbinoba Kevwe Charles *****

* (Department of Electrical and Electronics Engineering, Federal University of Petroleum Resources, P.M.B. 1221, Effurun, Delta State, Nigeria.)

** (Department of Electrical and Electronics Engineering, University of Benin, P.M.B. 1154, Benin City, Edo State, Nigeria.)

*** (Department of Electrical and Electronics Engineering, University of Benin, P.M.B. 1154, Benin City, Edo State, Nigeria)

## ABSTRACT

**This paper deals with the design of the Maximum Power Point Tracker (MPPT) and Phase Locked Loop (PLL) controllers in a PV-Inverter. The methods to optimizing the load of the PV module in order to capture the highest amount of energy, despite that the solar irradiation and cell temperature never is constant. Four types of Maximum Power Point Trackers (MPPT) have been discussed and a novel MPPT algorithm has been developed. The tracking of the fundamental grid voltage, by means of a Phase Locked Loop (PLL) was discussed. All the controllers have been designed by standard design techniques, and verified by simulation in MATLAB® / SIMULINK® and PSIM®.**

***Keywords*** **– Constant fill-factor, controllers, incremental conductance, sweeping, tracking.**

## 1. Introduction

The design of a power-electronic inverter depends on many issues, such as silicon devices; magnetics; capacitors; gate drives; grid performance; current-, voltage- and temperature-sensing and -protection; control strategies; and implementation, etc. This paper discusses two of the controllers for a PV-Inverter, this includes: Maximum Power Point Tracker (MPPT) for the PV module, Phase Locked Loop (PLL) to track the fundamental component of the grid voltage. There are other controllers in a PV-Inverter but not discussed in this paper. All the controllers needed in a PV-Inverter are illustrated in Fig. 1.

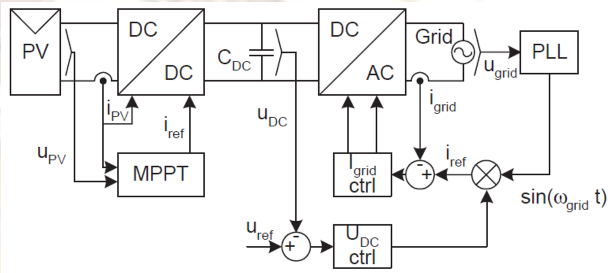

**Fig. 1:** Block diagram of the inverter with different control structures.

The controllers are hosted in an Interrupt Service Routine (ISR) running at 10.7 kHz, which also is the switching frequency. The ISR is running on an Infineon C167 CS-LM microcontroller, with a 25 MHz clock-frequency, Pulse Width Modulator (PWM), and 16 multiplexed 10-bit ADC channels.

The methods to optimizing the load of the PV module in order to capture the highest amount of energy, despite that the solar irradiation and cell temperature never is constant. Four types of Maximum Power Point Trackers (MPPT) have been discussed and a novel MPPT algorithm has been developed, to overcome some of the shortages with the present algorithms. Also, the tracking of the fundamental grid voltage, by means of a Phase Locked Loop (PLL), in order to synchronize the inverter to the grid, and to generate a high quality waveform-reference for the grid current. The detection of islanding operation by means of voltage and frequency monitoring. The frequency deviation is obtained from the PLL and the grid voltage is monitored by its RMS value. All the controllers have been designed by standard design techniques, and verified by simulation in MATLAB® / SIMULINK® and PSIM®.

## 2. Maximum Power Point Tracker (MPPT)

The operating point where the PV module generates the most power is denoted the Maximum Power Point (MPP) which co-ordinates are: UMPP, IMPP. The available power from the PV module is a function of solar irradiation, module temperature, and amount of partial shadow. Thus, the MPP is never constant but varies all the time. Sometimes it changes rapidly due to fast changes in the weather conditions (The irradiance can change as much as 500 W / ($m^2$ s), or from zero to bright sunlight in 2 seconds. This is measured during springtime 2005 with a pyranometer). At other times, it is fairly constant when no clouds are present. Four major types of tracking algorithms (MPPT) are available. They are (in order of complexity, simplest first):

- Constant fill-factor (voltage or current)
- Sweeping
- Perturb and observe (hill-climbing)
- Incremental conductance

Other types of algorithms also exist, e.g. fuzzy-logic, neural-networks, monitor/reference cells, etc. They are however not reviewed here, due to their elevated complexities, or the need for additional PV cells for monitoring purpose.

### 2.1 Constant Fill-Factor

The constant fill-factor algorithms assume that the MPP voltage is given as a constant fraction of the open circuit module voltage, $U_{OC}$, or that the MPP current is given as a constant fraction of the short circuit module current, $I_{SC}$ [1], [2]. These fractions are denoted the fill-factors, i.e. (and typical values):

$$FF_U = \frac{U_{MPP}}{U_{OC}} = 0.8 \quad (1)$$

$$FF_I = \frac{I_{MPP}}{I_{SC}} = 0.9 \quad (2)$$

and are assumed constant for all PV-modules, cell temperatures and solar irradiations.

2.1.1 Mode of operation

It is assumed that the PV module is operated at a given point. The MPPT algorithm turns off the converter for a short duration, e.g. 10 ms, and reads the open circuit voltage or the short circuit current. The reference for the module-voltage or -current for the next operating period, e.g. 1 second, is then given by the (1) or (2), with an assumed fill-factor.

The algorithm is easy to implement in the ISR. On the other hand, it includes two serious limitations. First, it assumes that the fill-factor is constant for all PV modules in the world, regardless of temperature and irradiation. This is, of course, not true. Second, rapid clouds may be present, thus the MPP may change faster than the 'normal operating period', 1 second in the foregoing example. This also leads to a lower generation than possible.

The fill factor for a given PV module and temperature can however be determined by scanning its voltage/current characteristics. This is done in [1] where the entire voltage/current characteristic is obtained by scanning the module in 25 ms, with a pause of several minutes in between. The actual fill factor, $FF_I$, is computed by (2) and stored for later use. The dynamic of the fill factor is very low so the pause of several minutes is not a problem. The obtained fill factor is then used to compute the current reference based on the short circuit current, which is recorded every 80 ms. This approach can also be used with the voltage fill factor, $FF_U$, but the relationship between the open circuit voltage and the MPP voltage is not as unique as for the current fill factor [3].

The largest disadvantage with this scheme is that the module must be short-circuited now and then (80 ms in [3]) in order to compute the actual fill factor and the current reference.

### 2.2 Sweeping

The basic sweeping algorithm is operating in a similar way as the constant fill-factor algorithm. As the name indicates, the algorithm performs a sweep in the modules power characteristic.

2.2.1 Mode of operation

It is assumed that the PV module is operated at a given point. The algorithm commands the converter to make a sweep in the modules characteristic. Simultaneously, the voltages and currents are recorded and the available power is calculated for each point. The point where the power is largest, the MPP, is stored and used as a new reference for the following period of normal operation, e.g. 1 second.

This algorithm is a little harder to implement in the ISR, due to the calculations of the power. Besides this, it must also include a comparator function in order to locate the MPP. The basic sweeping algorithm suffers from the same limitation as the constant fill-factor algorithm: Rapid clouds may be present, thus the MPP may change faster than the ‘normal operating period’.

Besides, if the sweep-duration is too long, the irradiance may have changed and the recorded curve corresponds to two different irradiations. This can be mitigated by starting the sweep at zero voltage, i.e. measuring the actual short circuit current. The sweep is then continued to open circuit conditions while all the different operating points are investigated for available power. Finally, the module is short circuited again and the new short-circuit currents are measured. Following, the irradiance has changed if the measured short-circuit currents do not agree with each other, and nothing can really be stated about the location of the MPP.

### 2.3 Perturb and Observer

The perturb-and-observe algorithm is also known as the ‘climbing hill’ approach. The reference is constantly changed, and the resulting power is compared with the previous power, and a decision about the direction of MPP can thus be stated [4].

2.3.1 Mode of operation

It is assumed that the PV module is operated at a given point. The voltage reference of the PV module is initialized to $U_{PV}$ *[n]. After the reference has been reached, the generated power $P_{PV}$[n] is calculated and stored. The reference is then changed to $U_{PV}$*[n+1], and the generated power, $P_{PV}$[n+1], is computed and stored. If $P_{PV}[n] > P_{PV}[n+1]$, the MPP is located in the opposite direction of which the reference was changed. Thus, the new reference should be equal to: $U_{PV}*[n+2] = U_{PV}*[n+1] - \Delta U$. In the opposite case where $P_{PV}[n] < P_{PV}[n+1]$, the MPP is located in the same direction as the change in the reference, and the new reference should be in the same direction: $U_{PV}$ $*[n+2] = U_{PV}*[n+1] + \Delta U$.

This way of searching in the MPP is fast when the irradiance is constant. On the other hand, it includes some limitations. First, the generated power is fluctuating around the MPP, while the PV voltage is alternating around the MPP. Making ΔU sufficiently small can mitigate this. However, this is on the cost of increasing the searching time when large variation in the irradiance is present. It is preferred to make ΔU large to catch the MPP during rapid changes, since the power loss due to the oscillations around the MPP is small. A large ΔU also enhances the signal-to-noise ratio in the sensed current.

Second, rapidly changing in the irradiation can lead to a wrong decision about the direction of the MPP [5]. This can however be solved by introducing a third reference, $U_{PV}$*[n+3], [6], [7]. Another solution is to ensure that the change in power as function of the change in the voltage-reference always is larger than the change in power due to change in radiation [8].

### 2.4 Incremental Conductance

The incremental conductance (IndCond) algorithm is based on the fact that the negative value of the instantaneous conductance ($-s_{PV} = -i_{PV}/u_{PV}$) and the incremental conductance ($ds_{PV} = di_{PV}/du_{PV}$), is equal at the MPP [5]. This is verified in (3):

$$
\begin{aligned}
&\frac{\partial\, p_{PV}}{\partial\, u_{PV}} = 0 \Leftrightarrow \\
&\frac{\partial\left(u_{PV}\cdot i_{PV}\right)}{\partial\, u_{PV}} = 0 \Leftrightarrow \\
&\frac{d\, u_{PV}}{d\, u_{PV}}\cdot i_{PV} + \frac{d\, i_{PV}}{d\, u_{PV}}\cdot u_{PV} = 0 \Leftrightarrow \\
&i_{PV} + \frac{d\, i_{PV}}{d\, u_{PV}}\cdot u_{PV} = 0 \Leftrightarrow \\
&\frac{d\, i_{PV}}{d\, u_{PV}} = -\frac{i_{PV}}{u_{PV}} \Leftrightarrow \\
&\frac{\Delta i_{PV}}{\Delta u_{PV}} = -\frac{i_{PV}}{u_{PV}}.
\end{aligned}
$$

(

3)

2.4.1 Mode of operation

It is assumed that the PV module is operated at a given point. The current and voltage are sampled and the differences are calculated as: Δi = i[n] - i[n-1] and Δu = u[n] - u[n-1], where [n] denotes the newly sampled values and [n-1] denotes the previous samples. If Δu is equal to zero, the sign on Δi is used to determine in which direction the MPP is located. If Δu is non-zero, the sign of Δi/Δu + I/U is used to determine the direction. The new current reference is then based on the previous reference plus the information about the direction. This is illustrated in Fig. 2.

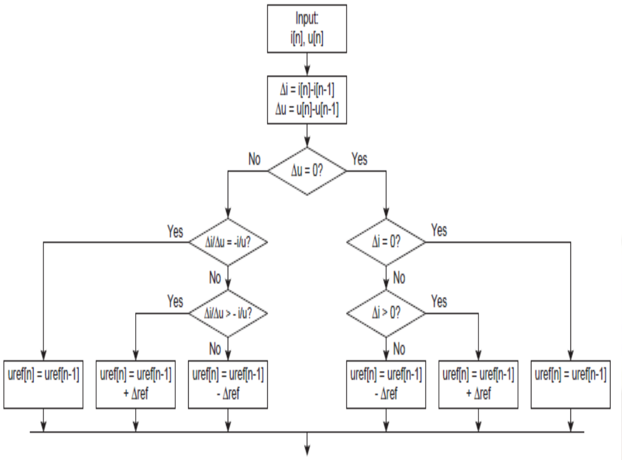

**Fig. 2:** Flow chart of the incremental conductance MPPT algorithm [5].

The algorithm is bypassed by the conditions: Δi = 0 and Δi/ Δu + i/u = 0, when the MPP is tracked, thus the power is no more fluctuating around the MPP.

The largest disadvantage with the IndCond algorithm, as with the other algorithms, is the problem of tracing the global maximum when the module is partial shadowed. Adding a scan mode to the algorithm can solve this. This is done in [9] where the voltage/current characteristic is scanned, during 40 ms, every 12 second, with a high amplitude signal to increase the signal-to-noise ratio. This also helps to increase the resolution of the sensed current, which can be a problem at low irradiance. The output from the scan is the co-ordinates for the global MPP, which then is used as the new reference before the IndCond algorithm is turned on again. This approach does not require any additional hardware. Another solution during partial shadowing is to make an initial estimation of $u_{MPP}/i_{MPP}$ as $(0.8 \times U_{OC})$ / $(0.9 \times I_{SC})$ [10], where $U_{OC}$ and $I_{SC}$ is monitored in the same way as in section 2.1. This helps to track the global MPP, even under severe partial shadow. However, this solution requires an additional circuit to perform the online estimation of $U_{OC}$ and $I_{SC}$. Some issues about digital implementation of the IndCond algorithm are given in [11].

### 2.5 Proposed MPPT

All the algorithms presented above include some disadvantages such as: erroneously detection of the MPP during rapid changes in the irradiation and under partial shadow; need for additional circuits for monitoring the closed loop current and open loop voltage; and fluctuation around the MPP. A solution is an extended sweep algorithm, presented in Fig. 3.

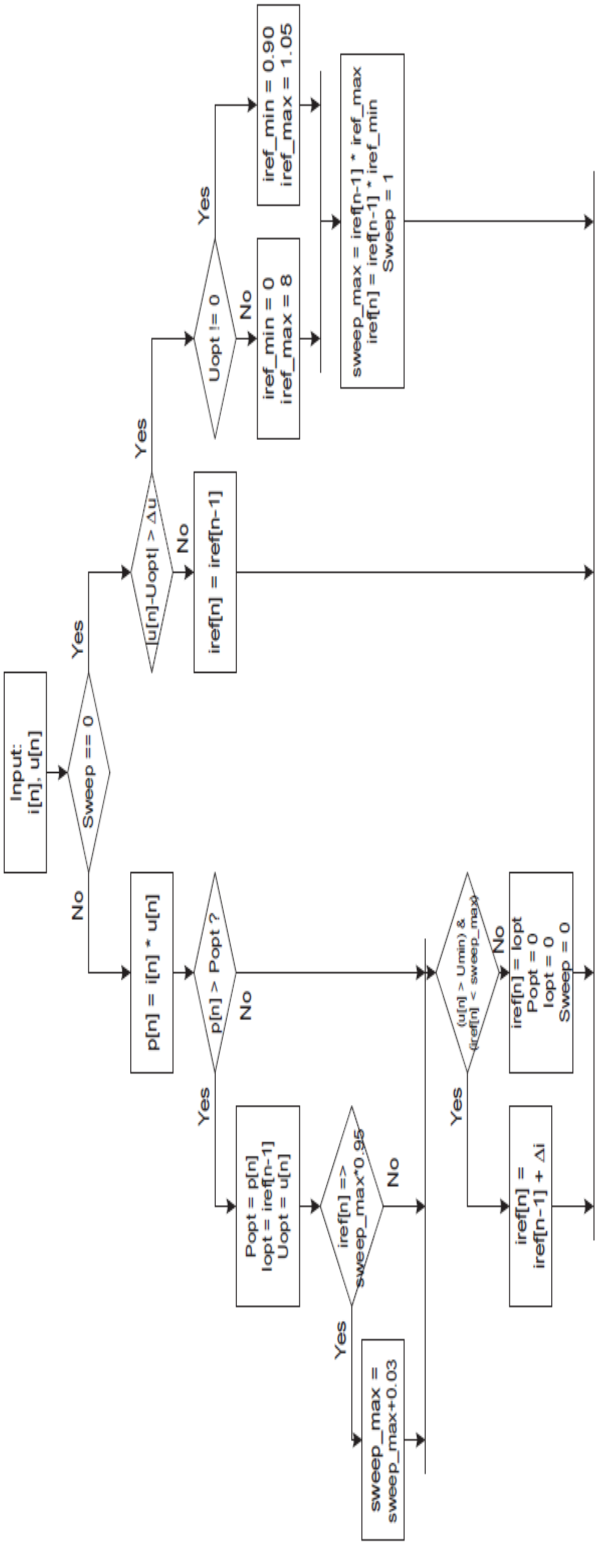

**Fig. 3:** Flow chart for the proposed MPPT.

2.5.1 Mode of operation

It is assumed that the PV module is operated at a given point. While this is on-going, the algorithm is monitoring the instantaneous module voltage, which should be equal to the recorded MPP voltage. Due to changes in temperature and/or irradiation, the instantaneous voltage will also change if the current is kept constant. Thus, instead of performing a new sweep every 10th second or so, a new sweep is only initialized when the module voltage has changed more than ΔU from the original MPP voltage. Moreover, the sweeping range is necessarily not equal to the entire module current range (from open circuit operation to the short circuit operation), but could be a fraction of the original MPP current, e.g. ΔI. This ensures a fast sweep, where only a little energy is lost.

The size of ΔU to start a new sweep is a tradeoff between power lost due to deviation from the real MPP during monitoring, and stability of the algorithm, i.e. how often the characteristic is swept. The change in the voltage across the module, $\Delta u_{PV}$, when the input current to the DC-DC converter is constant and the short circuit current is changed by an amount of $\Delta i_{SC}$, is:

$$\Delta u_{PV} \approx \frac{U_{MPP}}{I_{MPP}} \cdot \Delta i_{SC} \qquad (4)$$

when operated in the nearby region of the MPP. The threshold value to initiate a new sweep is set to 3% of the actual MPP current, which involves that sweep-mode is entered when the voltage has changed more than 3% from the previous MPP voltage.

The sweeping range is merely selected to be equal to $0.90\times I_{MPP}$ to $1.05\times I_{MPP}$, but is increased by additional 0.03 if the recorded power in the last sweeping-point exceeds the power in the next-last point. This is done to ensure that the MPP always will be tracked during the sweep. An Under-Voltage-Lock-Out (UVLO) is also included in the algorithm, not illustrated in Fig. 3, which decreases the current reference to 0.90 if the PV module voltage decreases below 20.0 V and starts the sweeping mode. This is to ensure than the voltage never collapses.

Finally, the algorithm must be able to follow the maximum rate-of-change-of-current, $di_{sc}/dt$, in order to track the MPP during rapid changes in the irradiation. The rate-of-change-of-current is proportional to the rate-of-change-of-irradiation, which is assumed to have a maximum value of 1000 $W/(m^2\times s)^6$. The STC short circuit current for modules is measured at 1000 $W/m^2$. Thus, the duration of the sweep, from zero-current and until the module voltage reached a predefined minimum, should not be larger than 1 second.

## 2.6 Simulated Results

The proposed MPPT algorithm is simulated in MATLAB/SIMULINK. The models of the PV module and the DC-DC converter are implemented in SIMULINK, together with the MPPT algorithm. The algorithm is programmed in C-code and compiled into an s-function for SIMULINK. The model of the PV module is based on the Shell Ultra175 module, operated at various irradiations but constant cell temperature. The temperature is kept constant, in order to make a simple prediction of the maximum available power for a given amount of irradiation.

The following is applied to all simulations: The function generating the normal distribution irradiation is sampled every 0.5s. The output from the normal distribution generator is multiplied with a noise-signal with mean 1.0 and variance $(0.01/3)^2$ (corresponds to a signal within the range from approx. 0.99 to 1.01). Finally, the irradiance is rate-limited to ± 1000 $W/(m^2\times s)$, in order to keep realistic rate-of-change-of-irradiance.

A simulation of increasing and decreasing irradiation is depicted in Fig. 4. Another set of eight simulations, with two different mean irradiations and four different variances are also made in order to evaluate the steady state efficiency of the MPPT algorithm at low and high irradiation. The results are presented in TABLE 1.

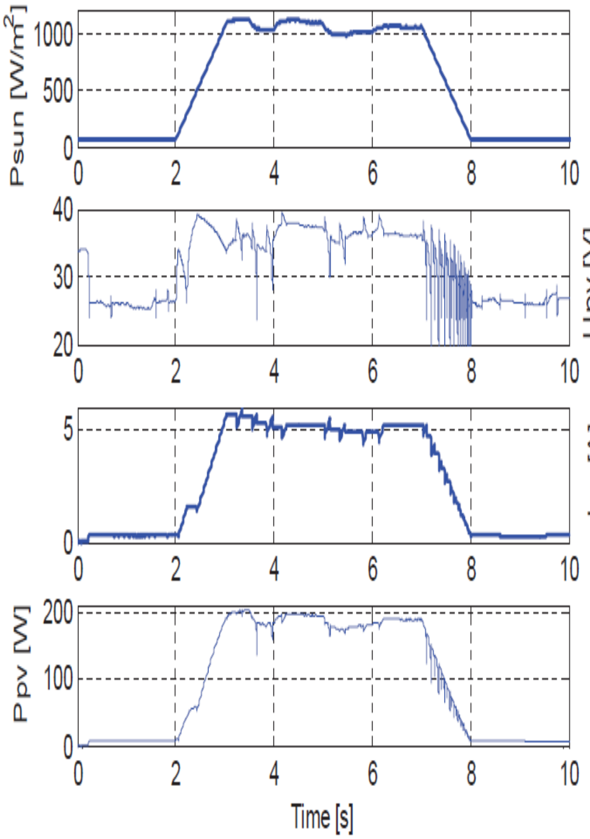

**Fig. 4:** Simulated results for the proposed MPPT algorithm.

The total efficiency is evaluated to 98.0%. From top and down: 1) Upper is shown the amount of solar irradiation. The high-level irradiation is defined in the span from 990 W/m2 to 1140 W/m2 in the time span from 3.0s to 7.0s. The low-level irradiation is approximately 60 W/m$^2$. 2) Voltage across the PV module. 3) Current drawn from the PV module. 4) Power generated by the PV module.

The total MPPT efficiency (simulated) in Fig. 4 is evaluated to 98.0%, and can be broken down to the following intervals ($P_{PV}/P_{MPP}$):

- Low irradiation (approx. 60 W/m$^2$): 28.5 J / 30.2 J = 94.3%,
- Increasing irradiation: 92.7 J / 99.5 J = 93.2%,
- High irradiation (approx. 1100 W/m$^2$): 741 J / 748 J = 99.1%,
- Decreasing irradiation: 92.4 J / 96.6 J = 95.7%.

This shows that the efficiency is good; both for low, high, increasing and decreasing irradiation.

The steady state performance evaluated in TABLE 1 shows that the proposed algorithm is capable of tracking the MPP with good accuracy, even though the irradiation is constantly changing (like the span from time = 3.0 s to 7.0 s in Fig. 4). The proposed MPPT algorithm is therefore considered designed.

**Table 1:** Simulated results for the proposed MPPT algorithm.

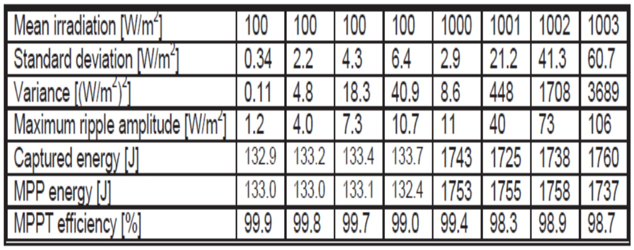

| Mean irradiation [W/m$^2$] | 100 | 100 | 100 | 100 | 1000 | 1001 | 1002 | 1003 |
|---|---|---|---|---|---|---|---|---|
| Standard deviation [W/m$^2$] | 0.34 | 2.2 | 4.3 | 6.4 | 2.9 | 21.2 | 41.3 | 60.7 |
| Variance [(W/m$^2$)$^2$] | 0.11 | 4.8 | 18.3 | 40.9 | 8.6 | 448 | 1708 | 3689 |
| Maximum ripple amplitude [W/m$^2$] | 1.2 | 4.0 | 7.3 | 10.7 | 11 | 40 | 73 | 106 |
| Captured energy [J] | 132.9 | 133.2 | 133.4 | 133.7 | 1743 | 1725 | 1738 | 1760 |
| MPP energy [J] | 133.0 | 133.0 | 133.1 | 132.4 | 1753 | 1755 | 1758 | 1737 |
| MPPT efficiency [%] | 99.9 | 99.8 | 99.7 | 99.0 | 99.4 | 98.3 | 98.9 | 98.7 |

## 3. Phase Locked Loop

The aim of the Phase Locked Loop (PLL) is to track the fundamental grid voltage, even though that severe background harmonics are present. Thus, the PLL can be regarded as a high-order band-pass filter, with zero phase distortion.

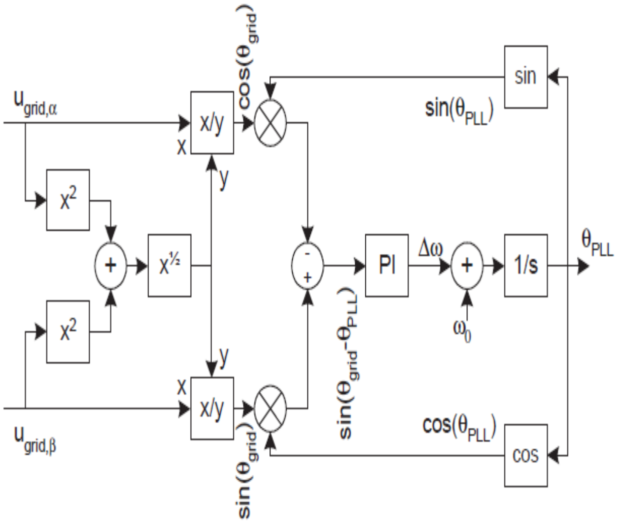

**Fig. 5:** Phase Locked Loop (PLL) used to synchronize a 3 phase dynamic voltage restorer with the grid in [12].

The basic structure of the PLL is shown in Fig. 5 [12]. However, [12] do not contain any information about how to tune the PLL structure.

The inputs to the structure are the a and b components of the grid-voltage, which is not possible for a single-phase grid. The output from the PLL is the fundamental sine wave. The structure uses a normalization of the grid amplitude. This is rather timeconsuming in the ISR, since it requires two multiplications, two divisions and a square-root operation. This is not necessary, since the amplitude is otherwise just included as a part of the proportional gain in the PI controller. A revised PLL structure is depicted in Fig. 6, where $\hat{U}_{grid,1}$ is the amplitude of the fundamental component at 50 Hz.

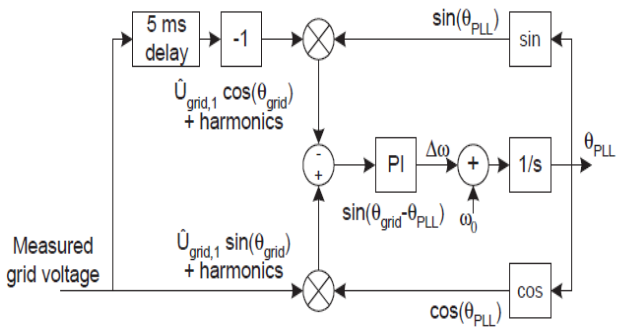

**Fig. 6:** Revised PLL structure (assuming a constant frequency of the grid voltage).

The error into the PI controller included in the PLL structure is given by inspection of Fig. 6 and assuming no harmonics and a constant frequency of 50 Hz:

$$err=\hat{u}_{grid}\cdot\sin(\theta_{grid})\cdot\cos(\theta_{PLL})-\hat{u}_{grid}\cdot\cos(\theta_{grid})\cdot\sin(\theta_{PLL})=\hat{u}_{grid}\cdot\sin(\theta_{grid}-\theta_{PLL})$$

(5)

where $\theta_{grid}$ and $\theta_{PLL}$ are the phase of the utility grid and the output of the PLL, respectively. The right-most equals-sign can be shown valid through the multiplication- and addition-formulas for trigonometric functions. The input to the PI controller is linearized around a working point, in order to tune the parameters within the PI controller.

Recognizing that error into the PI controller ($\theta_{grid}$ - $\theta_{PLL}$) is equal to zero at steady state operation, the linearized error into the PI controller can be described by a Taylor series as:

$$f(x)\approx f(X_0)+f'(X_0)\cdot(x-X_0)\Leftrightarrow \sin(x)\big|_{x=0}=\cos(0)\cdot(x-0)=x$$

(6)

Thus, the error into the PI controller becomes:

$$err\approx\hat{u}_{grid}\cdot(\theta_{grid}-\theta_{PLL})$$

(7)

The linearized small-signal transfer function of the PLL is:

$$PLL(s)=\frac{\hat{u}_{grid}\cdot PI(s)\cdot\frac{1}{s}}{1+\hat{u}_{grid}\cdot PI(s)\cdot\frac{1}{s}}=\frac{\hat{u}_{grid}\cdot PI(s)}{s+\hat{u}_{grid}\cdot PI(s)}=\frac{\frac{\hat{u}_{grid}\cdot Kp}{T_i}\cdot(T_i\cdot s+1)}{s^2+\hat{u}_{grid}\cdot K_p\cdot s+\frac{\hat{u}_{grid}\cdot K_p}{T_i}}$$

(8)

which is a typical second order system with one real zero. $K_p$ is the proportional gain, and $T_i$ is the integrator time constant. The natural frequency and damping can thus be stated as:

$$\omega_n=\sqrt{\frac{\hat{u}_{grid}\cdot K_p}{T_i}}$$

(9)

$$\xi=\sqrt{\frac{\hat{u}_{grid}\cdot T_i\cdot K_p}{4}}$$

(10)

An optimal damping ratio in terms of rise time and overshoot is known to be √½ [13]. Moreover, the relationship between the natural frequency and the rise time for a second order system (without zeros) is known to be [13]:

$$t_r\approx\frac{1.8}{\omega_n}$$

(11)

The parameters describing the PI controller can then be specified in terms of rise time, and grid voltage amplitude:

$$T_i\approx\frac{\sqrt{2}}{\omega_n}\approx 0.79\cdot t_r$$

(12)

$$Kp\approx\frac{\omega_n\cdot\sqrt{2}}{\hat{u}_{grid}}\approx\frac{2.55}{t_r\cdot\hat{u}_{grid}}$$

(13)

For a rise time of 10 ms, with optimal damping and European systems, the parameters of the PI controller equals: $K_p = 0.78$, and $T_i = 7.9\times10^{-3}$. A Bode plot is shown in Fig. 7 for different values of the amplitude of the grid voltage, $\hat{u}_{grid}$, and fixed controller parameters.

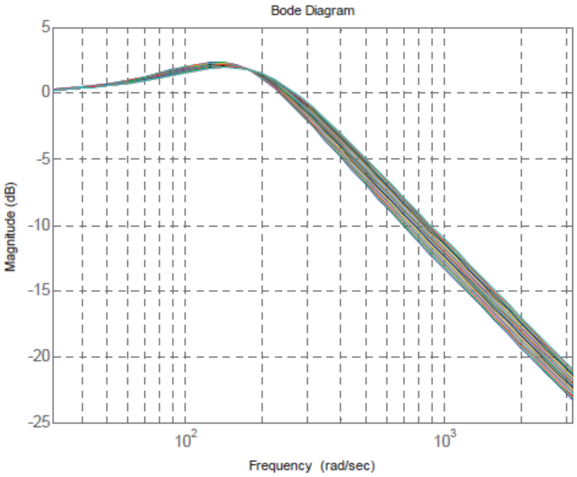

**Fig. 7:** Bode plot of the closed loop transfer function, when the peak grid voltage is swept from 275 V to 360 V. Controller parameters: Kp = 0.783, and Ti = 7.86×10-3, x-axis span: 5 Hz to 500 Hz.

The cosine-component of the grid voltage, $\cos(\theta_{grid})$, is computed by delaying the measured grid voltage, $\sin(\theta_{grid})$, with 90° (corresponds to 5 ms at 50 Hz) and multiplying the result with –1, cf. Fig. 6. Differentiating or integrating the measured grid voltage could also estimate the cosine component. The delay procedure is also used to compute the cosine component of the PLL output. This is done to reduce the phase error at frequencies different from 50 Hz (the 90 degree phase in the delay block).

If the 90° phase of the delay is incorrect, i.e. the grid frequency differs from the nominal 50 Hz, the output from the 5 ms delay-block in Fig. 6 is $\cos(\theta_{grid}) + A \times \sin(\theta_{grid})$. Assuming that a cosine trigonometric function is used to compute the $\cos(\theta_{PLL})$ , the error into the PI controller then becomes:

$$err,\cos = \hat{u}_{grid}\cdot\sin(\theta_{grid})\cdot\cos(\theta_{PLL}) - \hat{u}_{grid}\cdot\left[\cos(\theta_{grid}) + A\cdot\sin(\theta_{grid})\right]\cdot\sin(\theta_{PLL})$$

$$= \hat{u}_{grid}\cdot\sin(\theta_{grid} - \theta_{PLL}) + \hat{u}_{grid}A\cdot\sin(\theta_{grid})\cdot\sin(\theta_{PLL})$$

(14)

which contains an additional AC component at $\omega_{grid} + \omega_{PLL}$ rad/s (the right-most part of the equation). On the other hand, if the cosine of the PLL is substituted with another 5 ms delay-block, the error into the PI controller becomes:

$$err,5ms = \hat{u}_{grid}\cdot\sin(\theta_{grid})\cdot\left[\cos(\theta_{PLL}) + A\cdot\sin(\theta_{PLL})\right] - \hat{u}_{grid}\cdot\left[\cos(\theta_{grid}) + A\cdot\sin(\theta_{grid})\right]\cdot\sin(\theta_{PLL})$$

$$= \hat{u}_{grid}\cdot\sin(\theta_{grid} - \theta_{PLL})$$

(15)

which is equal to the result in (5). Thus the errors cancel each other, and no oscillations are present. This is also verified in Fig. 8 and Fig. 9.

The PI controller and integrator for the PLL are implemented in discrete time by emulation.

### 3.1 Simulated Results

Three events are simulated in the first simulation, cf. Fig. 8, Fig. 9 and Fig. 10. They are: voltage jumps from 230 V to 196 V, to 253 V and back to 230 V; phase jumps from 0° to -30°, to +30° and back to 0°, and frequency jumps from 50 Hz to 48 Hz, to 52 Hz, and back to 50 Hz. Both implementations of $\cos(\theta_{PLL})$ is shown, in order to evaluate the theory given above. Each of the components in the grid voltage is given as:

$$u_{grid,n} = \hat{U}_{grid,n}\cdot\sin(\theta_{grid,n})$$

$$\theta_{grid,n} = \int n\cdot\omega_{grid}\,dt + \theta_{grid,0}$$

(16)

where $u_{grid,n}$ is the time value of the $n^{th}$ component, $\hat{U}_{grid,n}$ is the amplitude of the $n^{th}$ component, $\theta_{grid,n}$ is phase of the $n^{th}$ component, $\omega_{grid}$ is the fundamental angular frequency of the grid, and $\theta_{grid,0}$ is the phase of the entire voltage.

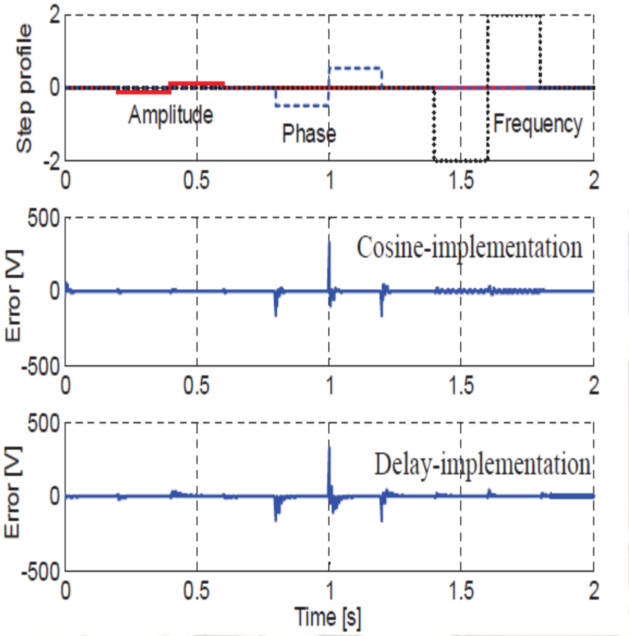

**Fig. 8:** Simulated results.

In Fig. 8, upper is the step profiles shown: voltage – 15% & 10%, phase:±30 degrees (±0.52 rad), frequency: ± 2 Hz. Middle is the error between the PLL output and the real grid, when a cosine is used in the PLL structure. Lowest is the error, when the cosine is replaced with a 5 ms delay block.

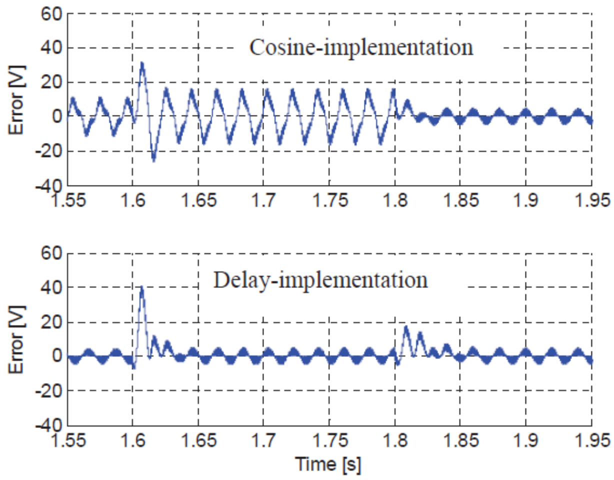

**Fig. 9:** Simulated results. Zoom of the two lower plots in Figure 8, from time = 1.55s to 1.95s.

The cosine implementation includes some oscillation in the output of the PLL when the grid frequency is shifted with ± 2 Hz. These oscillations are not seen in the delay-implementation.

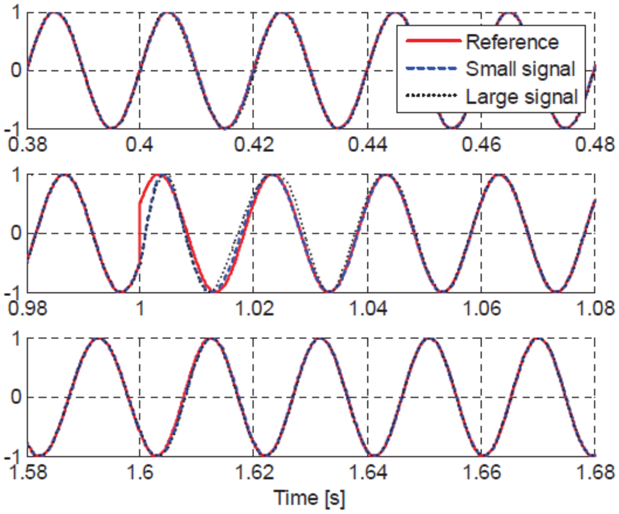

**Fig. 10:** Simulated results for the PLL small-signal and large-signal models (steps in amplitude, phase, and frequency according to Fig. 8).

The solid lines are the fundamental from the grid, which is used as reference. The dashed lines are from a small-signal model based on (8). The dotted lines are from the large-signal model in Fig. 6, also implemented in discrete time and with the 5 ms delay. The simulation reveals that an AC component is present in the difference between the output of the PLL and the fundamental of the grid (the error into the PI controller), when a cosine-trigonometric function is used to compute cos($\theta_{PLL}$). This is best seen in Fig. 9. The AC component is removed when the cosine-function is substituted with the delay-approach. The results in Fig. 10 show that the developed small-signal model in (8) agrees with the large-signal model in Fig. 6.

## 4. Detection of Islanding Operation

A simple islanding detection scheme is implemented in the inverter. The grid voltage must be within 230 V $\pm^{10\%}_{15\%}$ and the grid frequency must be within 50 ± 2 Hz. The inverter must cease injecting power into the grid, within 0.1 second, if these limits are broken.

**Table 2:** Simulated voltage harmonics in the grid. RMS value of fundamental component = 230.0 V, RMS value of all components = 231.3 V, and THD = 10.5%

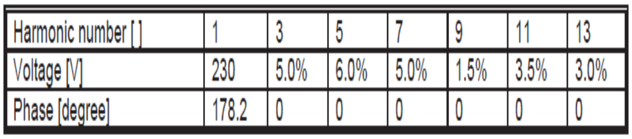

| Harmonic number [ ] | 1 | 3 | 5 | 7 | 9 | 11 | 13 |
|---|---|---|---|---|---|---|---|
| Voltage [V] | 230 | 5.0% | 6.0% | 5.0% | 1.5% | 3.5% | 3.0% |
| Phase [degree] | 178.2 | 0 | 0 | 0 | 0 | 0 | 0 |

The grid voltage can be monitored in many different ways: Average of the absolute grid voltage, Root Means Square (RMS) of the grid voltage, amplitude detection of the grid voltage by using the $\sin^2(x) + \cos^2(x) = 1$ relationship, and Fourier sine-transform of the grid voltage:

$$\left\langle \left| U_{grid} \right| \right\rangle_{20ms} = \frac{1}{20ms} \cdot \int_{0}^{20ms} \left| u_{grid} \right| dt \tag{17}$$

$$\left( U_{grid} \right)^2 = \frac{1}{20ms} \cdot \int_{0}^{20ms} \left( u_{grid} \right)^2 dt \tag{18}$$

$$\left( \hat{U}_{grid} \right)^2 = \left( u_{grid} \right)^2 + \left( delay\left( u_{grid}, 5ms \right) \right)^2 \tag{19}$$

$$\hat{U}_{grid} = \frac{2}{20ms} \cdot \int_{0}^{20ms} u_{grid} \cdot \sin\left( \theta_{PLL} \right) dt \tag{20}$$

Simulations are used to evaluate all four algorithms.

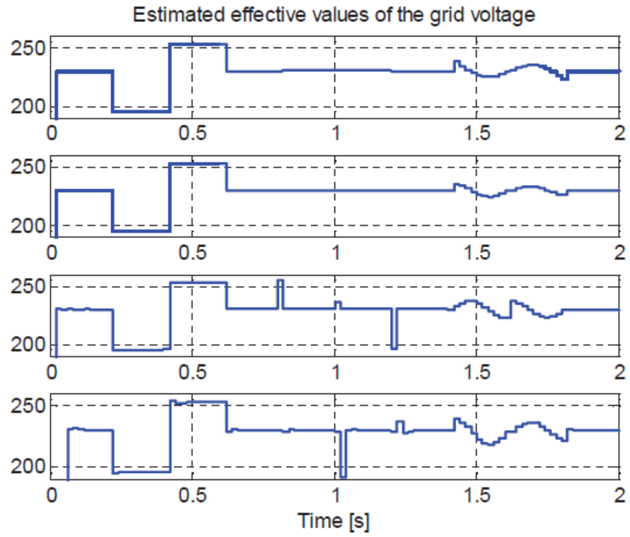

**Fig. 11:** Simulated results. The grid voltage is equal to the one in Fig. 8, which contains steps in amplitude, phase and frequency. From top and down: Average of absolute grid voltage, Root mean square, sin-cosine relationship, and Fourier sine-transform.

The results in Fig. 11 are for shifts in grid-amplitude, -phase and -frequency, without harmonics, like in Fig. 8. All four algorithms are detecting the correct value when amplitude jumps are present, but all are having troubles with detecting the correct values (and RMS value of 230 V) when the frequency is shifted. This is caused by the fact that the correct time of integration no more is equal to 20 ms, or that the correct delay time no more is equal to 5 ms. The last two algorithms have slight problems in detecting the correct value during the phase jump, but they obtain correct values after the transients.

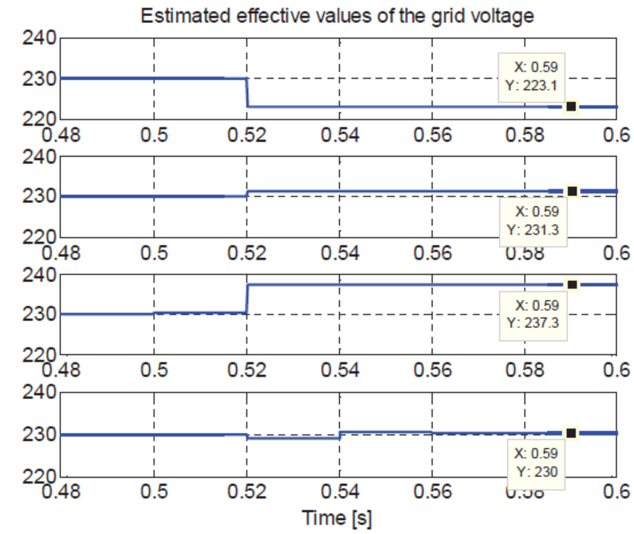

**Fig. 12:** Simulated results.

In Fig. 12, the grid voltage is equal to the one in TABLE 2, which contains many harmonics. The harmonics are turned on at time = 0.50 s. The RMS value is equal to 230.0 V before the harmonics are turned on, and 231.3 V after. From top and down: Average of absolute grid voltage, Root mean square, sin-cosine relationship, and Fourier sine transform.

The results in Fig. 12 are when severe harmonics are present in the grid voltage, according to TABLE 2. Only the RMS and the Fourier sine-transform algorithms succeed in estimating the correct values. The averaging algorithm underestimates the value and the sin-cosine relationship algorithm overestimates it.

The averaging algorithm is far the easiest to implement in the ISR since it only requires an integrator. The RMS and the Fourier sine-transform algorithms are a little more demanding, since they do also require a multiplication of two time-varying signals. Finally, the sin-cosine relationship algorithm requires a 5 ms delay of the sampled signal and two multiplications (the delay is already included in the PLL), or a 5 ms delay of the sampled signal, raised to the second power (not included in the PLL). Taking all these issues into consideration, the RMS algorithm seems to be the best candidate for detecting the level of voltage, both in term of precision and implementation.

The frequency of the grid is monitored by the output of the PI controller included in the PLL structure. The output of the PI controller is equal to the difference between the actual frequency and the nominal frequency ($\omega_0$ in Fig. 6). The output from the calculation of the RMS value of the grid voltage, and the output from the PI controller are both fed to a detection circuit similar to the one illustrated in Fig. 13. The purpose of the circuit is to detect if its input parameter is outside the premised range. The output signal of the circuit goes low, indicating an islanding situation, if the input signal exceeded the limit in more than 0.1 second. This is done to avoid nuance tripping of the inverter, in case of the normal dynamics events (phase and amplitude jumps) in the grid.

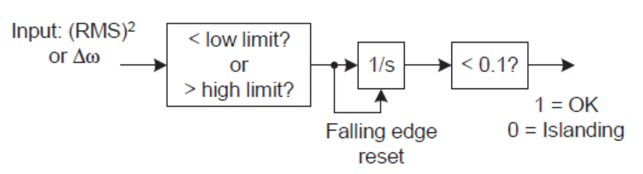

**Fig. 13:** Islanding detection circuit for the RMS value or frequency of the grid voltage. The input signal must be outside its limits in least 0.1 second, before the inverter is stopped, this to avoid nuance tripping. The limits in the right-most block are equal to (230 V × 0.85)2 and (230 V × 1.10)2. The limits are substituted with ± 2×2π for the frequency monitoring scheme.

## 5. Conclusion

The design of the Maximum Power Point Tracker (MPPT) and Phase Locked Loop (PLL) controllers in a PV-Inverter has been discussed. The methods to optimizing the load of the PV module in order to capture the highest amount of energy despite that the solar irradiation and cell temperature never is constant was also discussed. Four types of Maximum Power Point Trackers (MPPT) have been discussed and a novel MPPT algorithm has been developed, to overcome some of the shortages with the present algorithms. Also, the tracking of the fundamental grid voltage, by means of a Phase Locked Loop (PLL), in order to synchronize the inverter to the grid, and to generate a high quality waveform-reference for the grid current. The detection of islanding operation by means of voltage and frequency monitoring. The frequency deviation is obtained from the PLL and the grid voltage is monitored by its RMS value. All the controllers have been designed by standard design techniques, and verified by simulation in MATLAB®/SIMULINK® and PSIM®.

## REFERENCES

[1] S. Yuvarajan, X. Shanguang, Photo-voltaic power converter with a simple maximum-power-point-tracker, *IEEE proc. of the 2003 international symposium on circuits and systems (ISCAS '03), vol. 3, 2003, 399-402.*

[2] J.H.R Enslin, M.S. Wolf, D.B. Snyman, W. Swiegers, Integrated photovoltaic maximum power point tracking converter, *IEEE trans. on industrial electronics, vol. 44, 1997, 769-773.*

[3] T. Noguchi, S. Togashi, R. Nakamoto, Short-current pulse-based maximumpower-point tracking method for multiple photovoltaic-and-converter module system, *IEEE trans. on industrial electronics, vol. 49, 2002, 217-223.*

[4] D.P. Hohm, M.E. Ropp, Comparative study of maximum power point tracking algorithms using an experimental, programmable, maximum power point tracking test bed, *IEEE proc. of the 28th photovoltaic specialists conference, 2000, 1699- 1702.*

[5] K. H. Hussein, I. Muta, T. Hoshino, M. Osakada, Maximum photovoltaic power tracking: an algorithm for rapidly changing atmospheric conditions, *IEE proc. of generation, transmission and distribution, vol. 142, 1995, 59-64.*

[6] M. Yamaguchi, K. Kawarabayashi, T. Takuma, Y. Ueda, Y. Yamano, Development of a new utility-connected photovoltaic inverter LINE BACK, *Proc. of the 16th international telecommunications energy conference (INTELEC'94), 1994, 676-682.*

[7] Y.-T. Hsiao, C.-H. Chen, Maximum power tracking for photovoltaic power system, *IEEE proc. of the 37th annual industry application conference (IAS'02), vol. 2, 2002, 1035-1040.*

[8] N. Femia, G. Petrone, G. Spagnuolo, M. Vitelli, Optimization of perturb and observe MPPT method, *IEEE trans. on P.E., 20(4), 2005, 963-973.*

[9] W. Wu, N. Pongratananukul, W. Qiu, K. Rustom, K. Kasparis, I. Batarseh, DSP-based multiple peak power tracking for expandable power system, *IEEE proc. of the 18th annual*

*applied power electronics conference and exposition (APEC'03), vol. 1, 2003, 525-530.*

[10] K. Kobayashi, I. Takano, Y. Sawada, A study on a two stage maximum power point tracking control of a photovoltaic system under partially shaded isolation conditions, *IEEE proc. of the power engineering society general meeting, vol. 4, 2003, 2612-2617.*

[11] T.-Y. Kim, H.-G. Ahn, S. K. Park, Y.-K. Lee, A novel maximum power point tracking control for photovoltaic power system under rapidly changing solar radiation, *IEEE proc. of the international symposium on industrial electronics (ISIE'01), vol. 2 , 2001, 1011-1014.*

[12] J.G. Nielsen, *Design and Control of a Dynamic Voltage Restorer*, Ph.D. thesis, Institute of Energy Technology, Aalborg University, 2002.

[13] G.F. Franklin, J.D. Powell, A. Emami-Naeini, *Feedback control of dynamic systems* 3rd edition, (Addison Wesley) ISBN: 0-201-53487-8.

[14] S.B. Kjaer, *Design and Control of an Inverter for Photovoltaic Applications*, Ph.D. thesis, Institute of Energy Technology, Aalborg University, 2005.